phys. stat. sol. (a) **150**, 51 (1995)

Subject classification: 61.16; 61.72; S1.3; S10

Max-Planck-Institut für Mikrostrukturphysik, Halle/Saale[1])

HREM Simulations of Ag Particles in Sodium Silicate Glasses Refined by Molecular Dynamic Relaxations

By

D. TIMPEL and K. SCHEERSCHMIDT

(Received May 10, 1995)

Dedicated to Professor Dr. JOHANNES HEYDENREICH on the occasion of his 65th birthday

Providing local information at an atomic level high resolution electron microscopy (HREM) is applied to investigate Ag particles in sodium silicate glasses. Here, the structure of the embedded metallic particles, which influence the properties of glasses, is described by molecular dynamics relaxation calculations. The possibility of HREM to vizualize the structural modifications owing to relaxations is discussed on the basis of simulated HREM micrographs.

Hochauflösende Elektronenmikroskopie (HREM) wird wegen der direkten atomaren Strukturabbildung zur Untersuchung von Ag-Teilchen in Natriumsilikat-Gläsern verwendet. Die Struktur der eingelagerten Metallteilchen, die wesentlichen Einfluß auf die Glaseigenschaften hat, wird dabei durch molekulardynamische Relaxationsrechnungen beschrieben. Die Möglichkeiten der Sichtbarmachung struktureller Veränderungen im HREM infolge der Relaxationseffekte werden anhand von computersimulierten Abbildungen diskutiert.

1. Introduction

Optical and electrical properties of glasses are strongly influenced by the formation of metallic inclusions. For example, crystalline Ag particles of nanometer size embedded in sodium silicate glasses cause a coloration of the glass depending, e.g., on particle size, shape, distribution, and penetration depth. The precipitates were generated by a sodium–silver ion exchange via the glass surface, thermally activated migration, and subsequent annealing. Commercial sodium silicate glasses (0.13% Fe_2O_3) are exposed to an ion exchange with a $NaNO_3/AgNO_3$ melt at 400 °C. Subsequent annealing at temperatures between 460 and 600 °C creates Ag particles up to 120 nm in size [1].

In dependence on annealing process and particle size experiments with such glasses suggest a behaviour of Ag precipitates in glass deviating from the bulk structure. In particular, high resolution electron microscope investigations (HREM, see Fig. 1: Ag particle of about 4 nm in diameter in sodium silicate glass), providing structural information at atomic level, indicate that with declining particle diameter the lattice parameters decrease more strongly than expected for free particles [2]. Structural models of sodium silicate glasses and embedded silver particles are generated by means of molecular dynamic and molecular static calculations to prove this effect, in particular the influence of the matrix on the particle

[1]) Weinberg 2, D-06120 Halle/Saale, Federal Republic of Germany.

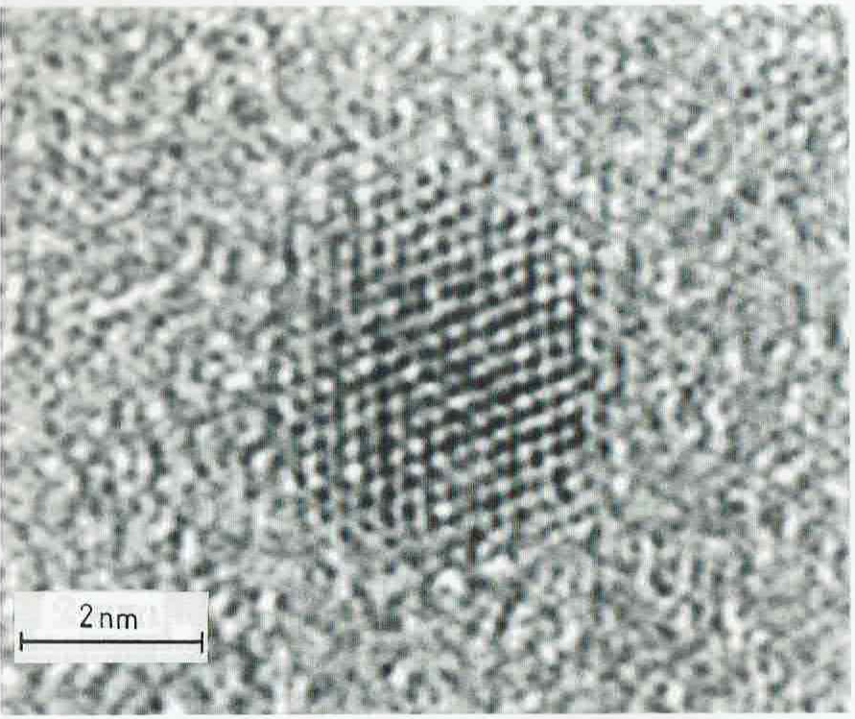

Fig. 1. (111) lattice fringes (U = 400 kV, HREM micrograph: H. Hofmeister, MPI Halle) of an Ag particle within commercial sodium silicate glass after ion exchange and annealing

relaxation. Furthermore, image simulations on the basis of such relaxed structure models are carried out to assess the possibilities of HREM to image small Ag particles in glass as well as the influence of the imaging process on the HREM micrographs [3, 4].

2. Molecular Dynamic Simulations of Ag in Glass

Extensive atomic level simulations are often based on empirical potentials describing the atomic interactions only as a function of the atomic positions. It is supposed that the total potential energy of an N-body system is represented by a combination of different N-body interactions or semiempirical mean field approximations. Depending on the properties of the system considered it is possible to neglect higher moments. Up to a certain degree, for ionic and pure van der Waals systems, an approximation only based on pair potentials seems to be sufficient. However, with increasing covalent or metallic bonding character it is necessary to include many-body potential terms. Metals are well described by embedded atomic potentials [5 to 7], whereas covalent structures demand special many-body potentials such as Stillinger-Weber potential [8], Tersoff potential [9, 10], or the modified Born-Mayer-Huggins pair potential including Stillinger-Weber angular terms [11].

To the computer-aided model generation and energy calculations the CERIUS [12] program package is applied. The total energy has to include the valence bonding, the

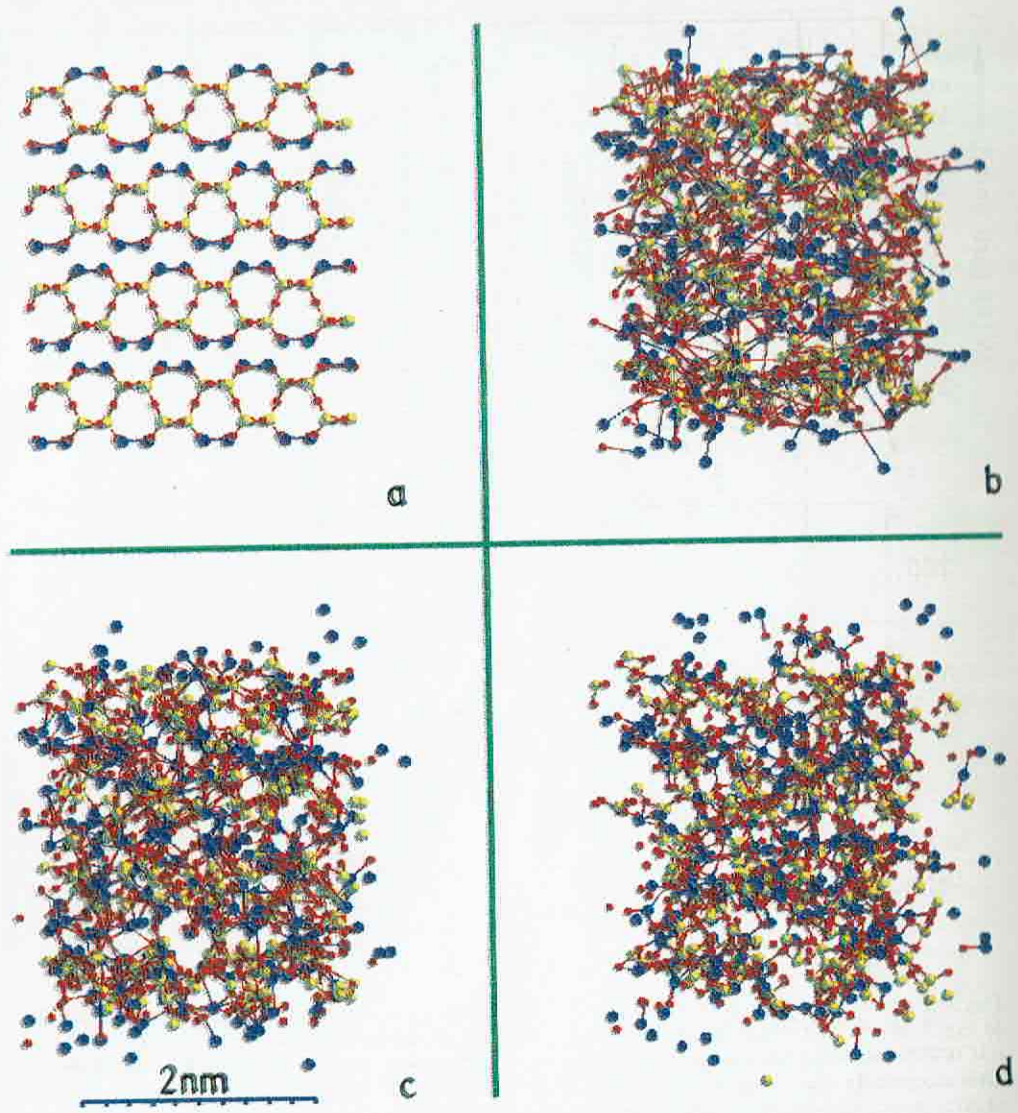

Fig. 2. Generation of models of a sodium silicate glass (sections of the $4 \times 2 \times 4$ supercell, [001] orientation shown): a) crystalline basis structure α-$Na_2Si_2O_5$, orthorhombic Pcnb, a = 0.6410 nm, b = 1.542 nm, c = 0.4896 nm, density = 2.514 g/cm^3; b) energy relaxation using Morse pair potentials and universal-force-field angular terms after statistically disturbing the atom positions (0.1 to 0.2 nm) and recalculating the bonding structure; c) 30% rearrangement of six-rings to five- and seven-rings of Si–O and subsequent energy relaxation; d) MD simulation, 20 ps at 2000 K, cooling down to 300 K, final density = 1.687 g/cm^3

three-, and four-body interactions, i.e. distance, angle, torsion, and inversion of the bonds and corresponding bonding strength. During energy minimization, owing to the negative

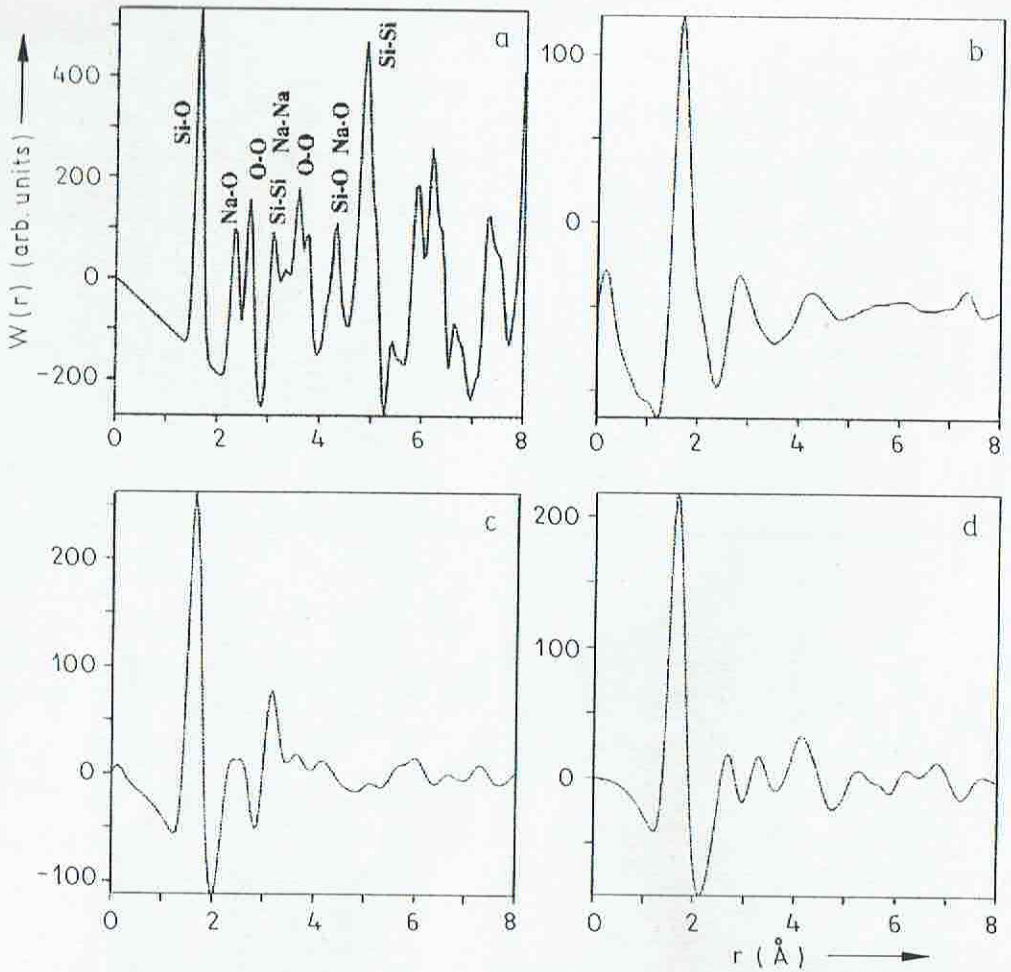

Fig. 3. Reduced pair distribution functions of the different sodium silicate structures corresponding to Fig. 2: a) crystalline basis structure α-$Na_2Si_2O_5$, orthorhombic Pcnb, $a = 0.6410$ nm, $b = 1.542$ nm, $c = 0.4896$ nm; b) energy relaxation using Morse pair potentials and universal-force-field angular terms after statistically disturbing the atom positions (0.1 to 0.2 nm) and recalculating the bonding structure; c) 30% rearrangement of six-rings to five- and seven-rings of Si–O and subsequent energy relaxation; d) MD simulation, 20 ps at 2000 K, cooling down to 300 K

the equations of motion. In order to describe the sodium silicate glass up to now Morse-like pair potentials are applied to the bond distance interaction, with a Fourier expansion describing the many-body angular term, whereas a 12–6 Lennard-Jones interaction is used for the metallic particle and its interface as well as all non-bonded interactions. The force field parameters (bonding length, angle, bonding strength, scaling factors) are fitted to the molecule properties as well as to get stable extended crystalline configurations which can be varied to cover all possibilities of the unknown data. The force field used here qualitatively reproduces the energy of the system, however, it fails in calculating the nearest neighbour

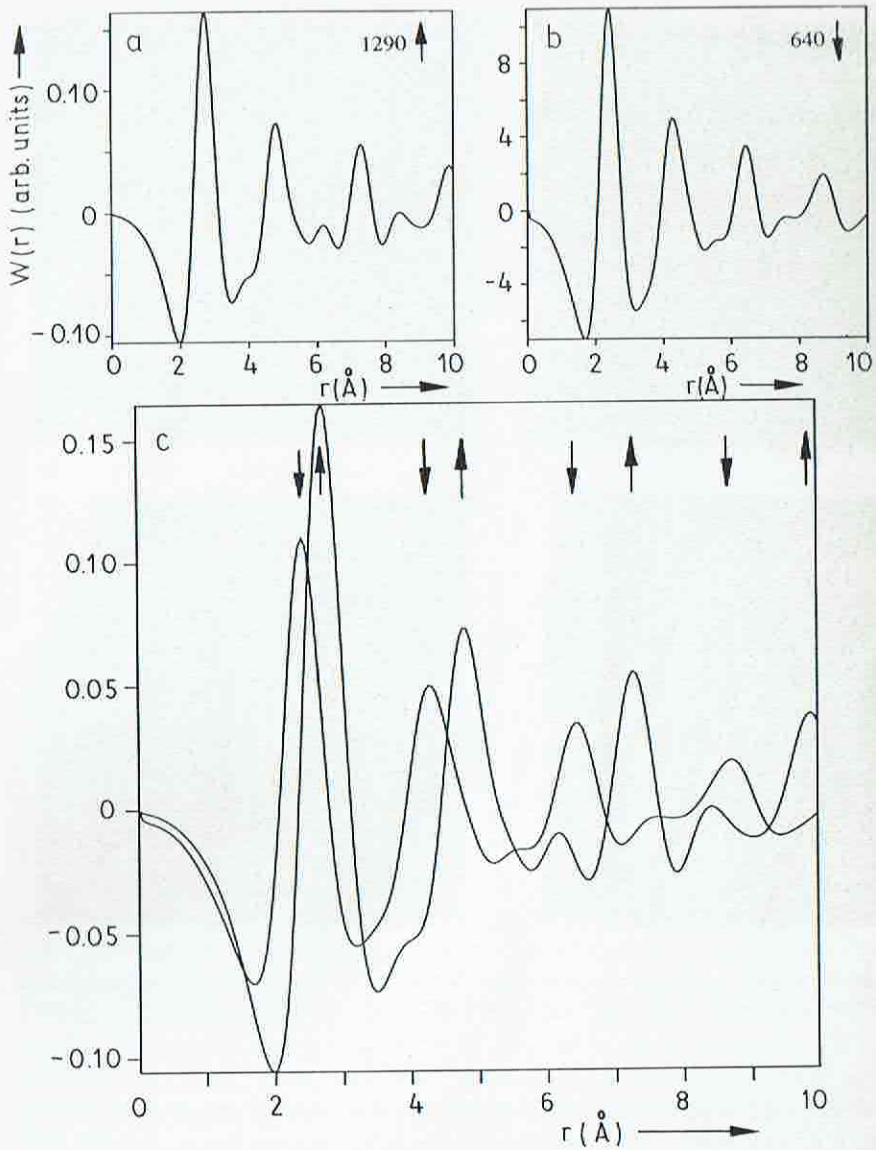

Fig. 5. Reduced partial Ag–Ag PDFs of two cuboctahedral particles; a) 1290 and b) 640 atoms sodium silicate glass after relaxation of the whole system; c) scaled comparison to demonstrate lowering and broadening of the lattice distances with decreasing particle size

above. First calculations using the Born-Mayer-Huggins pair potential with Stillinger-We angular terms [11] and different algorithms show differences in the details and will reflected elsewhere.

In order to construct a realistic glass model (random network model), an amorph structure in local atomic environment like a crystal, with the correlation of the ato

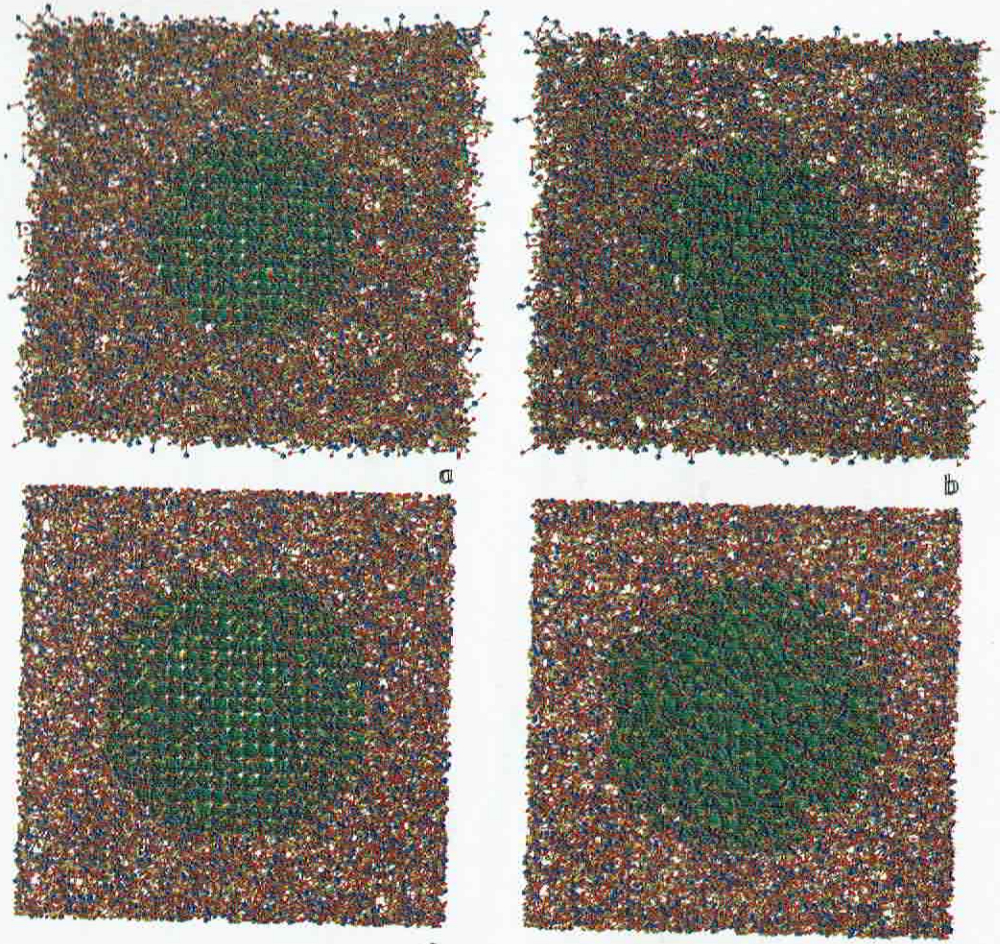

Fig. 4. a), c) Unrelaxed and b), d) relaxed model of a spherical (a), b) 857 atoms) and a cuboctahedral (c) d) 1290 atoms) Ag particle in the $10 \times 4 \times 12$ sodium silicate glass matrix ($6.4 \times 6.2 \times 5.8$ nm^3)

Different strategies are considered in order to generate such a glass. The first method starts with the statistical disturbance of the atomic positions of the sodium silicate crystal. After bond reordering, only depending on the interatomic distances, the structure will relax. In the second method, the bonding relations of the crystal are directly manipulated by statistically converting a sufficient rate of the six-fold Si–O rings to five- and seven-fold ones, followed by energy minimization [13]. Besides, MD calculations offer a third possibility of generating a glass model by annealing treatments at sufficiently high temperatures. In most cases the first method is chosen in spite of topological disadvantages. Huge structures of about 16000 atoms could not yet be modelled by means of other methods. Fig. 2 compares different glass models and the starting point of each simulation, i.e. an α-$Na_2Si_2O_5$ crystal (Fig. 2a). Energy minimization after statistically disturbing the crystalline

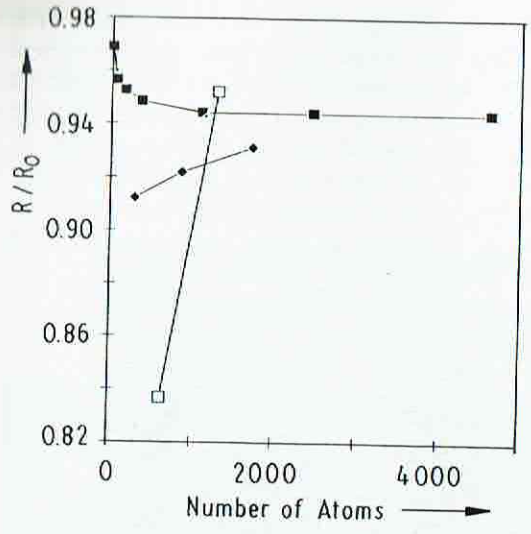

Fig. 6. Variation of the next neighbour tance of free particles (■) as well as of cubo hedral (□) and spherical (◆) Ag particle sodium silicate glass in dependence on part size

correlations of the atomic positions va ishing over long distances but topolo cally inadequately describing the lo environment. A rearranging of the cr talline six-fold ring structure and su sequent relaxation avoid topological m takes (Fig. 2c). A sodium silicate gl generated by MD calculations is sho in Fig. 2d. Fig. 3 presents the pair d tribution functions (PDFs) correspon ing to Fig. 2, which characterize the amorphous structure in dependence on the relaxati behaviour and the structure modelling. Compared with the peaks of the crystal (Fig. 3 the peaks of the glass structures are lowered and broadened. Solely for small distanc these structures reveal a correlation of the atomic position. Crystalline silver particles different shape (cuboidol, cuboctahedral, and spherical) and size (200 to 2000 atoms) a included in enlarged sodium silicate glasses ($6.4 \times 6.2 \times 5.4$ nm^3, 15840 atoms) with t whole system being relaxed again (Fig. 4). As mentioned above the Ag interacts v Lennard-Jones potentials with Ag and all particles of the glass matrix. The unrelaxe (Fig. 4a, c) and the relaxed (Fig. 4b, d) states of two Ag precipitates (Fig. 4a, b spherica Fig. 4c, d cuboctahedral), which are included in a sodium silicate glass, are given, revealin small displacements of the surface atoms of the relaxed particle. A comparison of the reduce partial Ag–Ag PDF of two embedded cuboctahedral silver particles of different size (64 and 1290 atoms) after relaxation give more detailed information on the relaxation behaviou of the precipitate and therefore on the influence of glass (see Fig. 5). Besides a lowering an a broadening of the crystal peaks in Fig. 5 there is a slight shift of the peak maxima toward smaller distances for the smaller particle. For comparison, different particle shapes an diameters as well as free silver particles — without surrounding glass matrix — are relaxe using potentials and parameters equivalent to the previous ones (see Fig. 6, details discusse later on).

3. HREM Image Simulations

The experimental HREM investigations are carried out in a JEOL-JEM4000EX near th Scherzer focus (50 nm) to obtain optimum contrast [2]. Fig. 1 shows a silver particle withi a sodium silicate glass, with the typical fringe contrast disturbed by an inner particl structure, probably owing to a lattice defect. The (111) lattice fringes characterizing th crystalline particle structure clearly stand out against the speckled contrast of the amorph

However, a direct and phenomenological interpretation of the HREM micrographs is mostly not possible so that image processing and image simulations with theoretical structure models are inevitable. The HREM image contrast is mainly determined by two processes: First, by the electron interferences owing to the interaction process of the electron beam with the almost periodic potential of the matter, and second, by the interference of the plane waves scattered by the specimen and transferred by the microscope. Images are modelled by calculating both processes. Starting from an initial model, imaging conditions and model have to be varied up to sufficient coincidence of simulated image and experimental contrast (trial and error). Both the CERIUS [12] and the EMS [16] multislice software are applied to simulate the image contrast. The

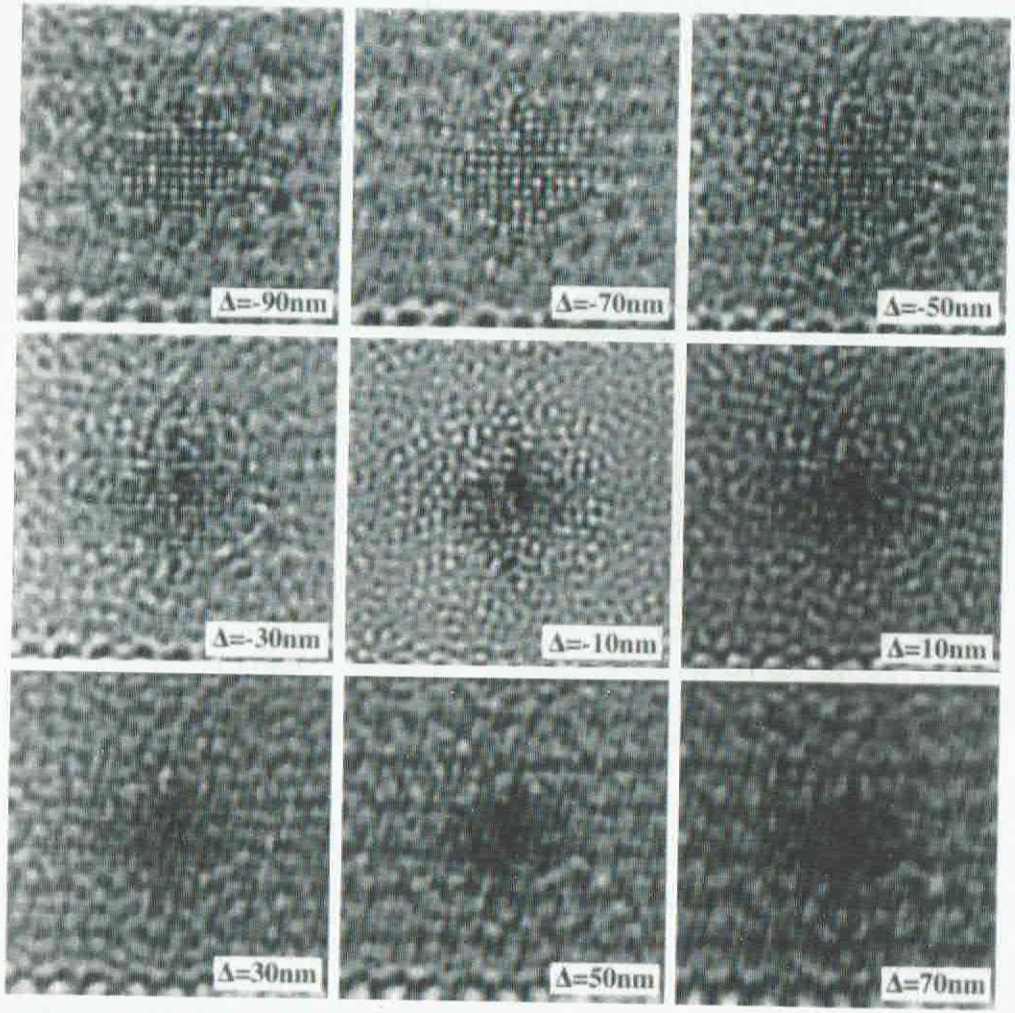

Fig. 7. Simulated HREM defocus series of the relaxed cuboctahedral (640 atoms) (100)-oriented Ag particle in the $10 \times 4 \times 12$ sodium silicate glass matrix at 400 kV, $C_s = 1$ mm, $\delta = 10$ nm, $\alpha = 0.5$ mrad

assumptions made for the microscope parameters are mostly related to the experim
i.e. accelerating voltage $U = 400$ kV, the spherical aberration $C_s = 1$ mm, the defocus sp
$\delta = 10$ nm, the semiangular beam divergence $\alpha = 0.5$ mrad, and the diffraction aper
$\alpha' = 16\ \mathrm{nm}^{-1}$.

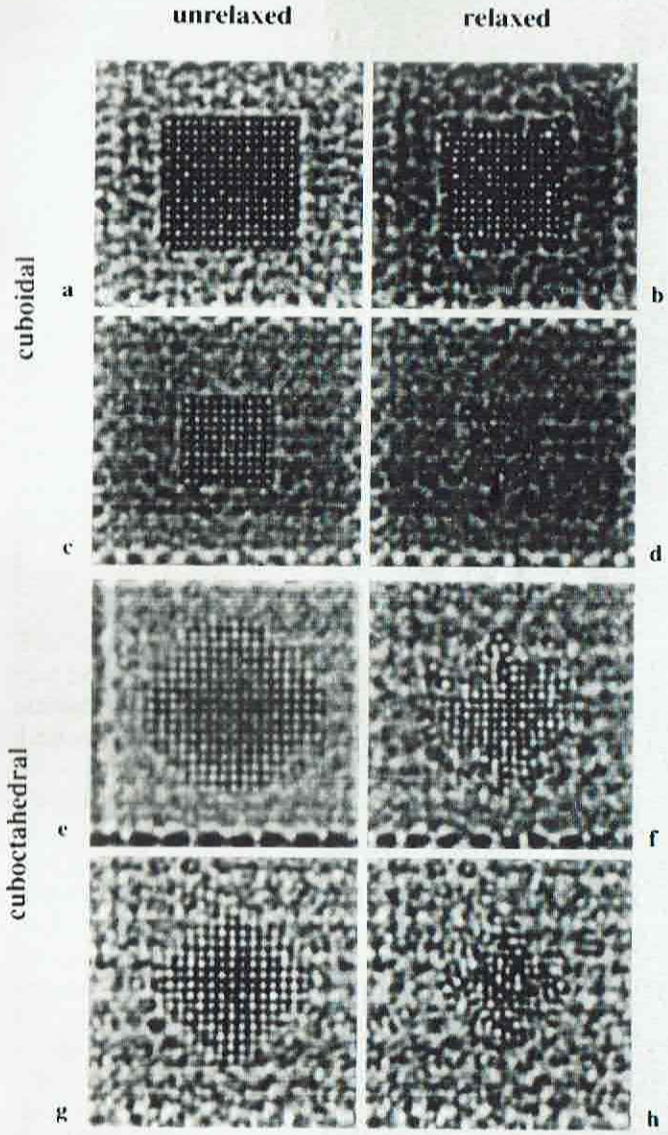

Fig. 8. HREM images simulated for different shapes, diameters and relaxations of the (100)-orie
Ag particle in the $10 \times 4 \times 12$ sodium silicate glass matrix: huge (a), b) 1372 atoms) and small (
666 atoms) cuboidal; hugh (e), f) 1290 atoms) and small (g), h) 640 atoms) cuboctahedral; a), c),
non-relaxed particle; b), d), f), h) whole system relaxed. Imaging parameters: $U = 400$ kV, $C_s = 1$

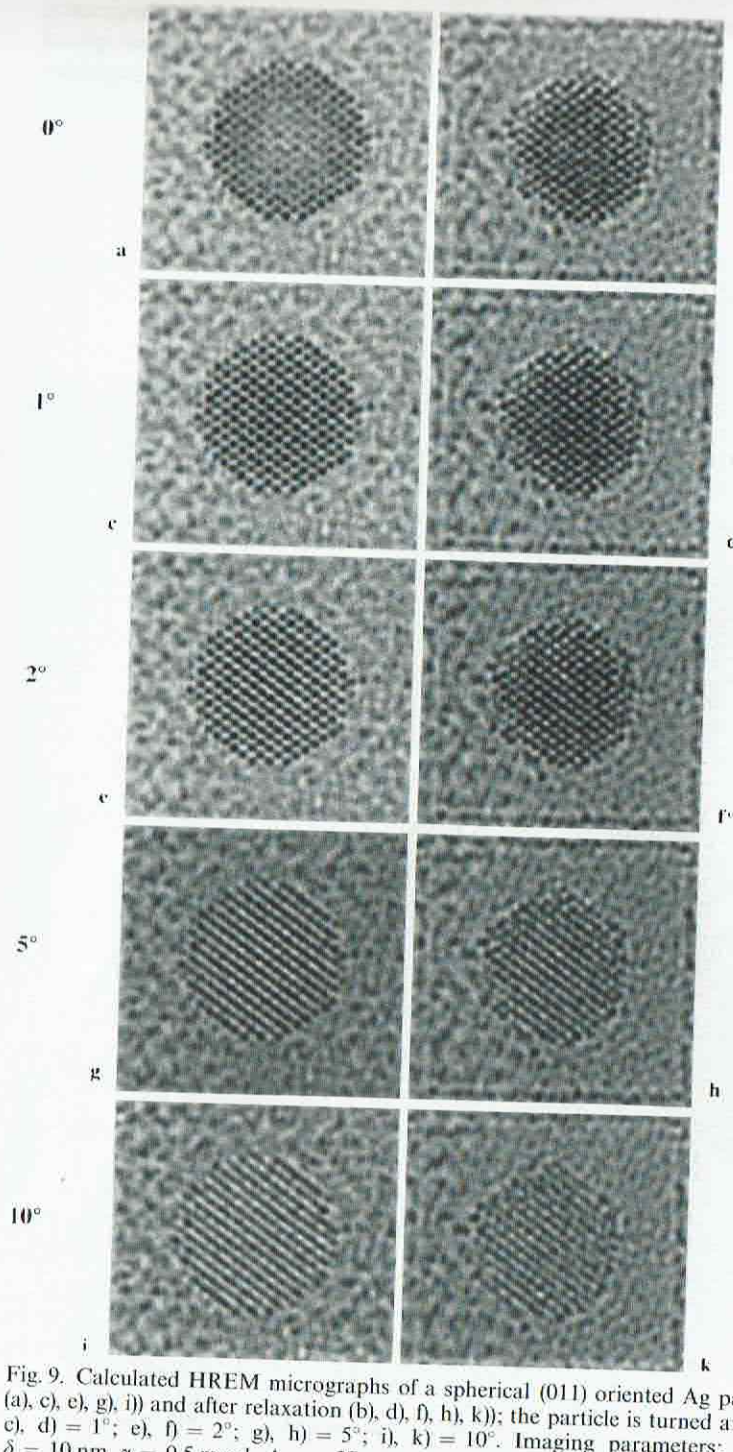

Fig. 9. Calculated HREM micrographs of a spherical (011) oriented Ag particle (1722 atoms) before (a), c), e), g), i)) and after relaxation (b), d), f), h), k)); the particle is turned around ($1\bar{1}1$) by a), b) = 0°; c), d) = 1°; e), f) = 2°; g), h) = 5°; i), k) = 10°. Imaging parameters: $U = 400$ kV, $C_s = 1$ mm, $\delta = 10$ nm, $\alpha = 0.5$ mrad, $\Delta = -37$ nm

For embedded silver particles of varying shape, size, relaxation state, and orien HREM micrographs are calculated. Fig. 7 presents a simulated HREM defocus seri cuboidal particle in (100) orientation after relaxation. In steps of 20 nm the defo increased from −90 nm underfocus to 70 nm overfocus. The Scherzer focus is at −40 nm, where a broad band of $\pi/2$ phase-shifted spatial frequencies is transf showing the pronounced speckled contrast of the amorphous matrix. The lattice fringes particle are clearly detectable at underfocus values lower than those of the Scherzer For overfocus the particle solely creates a dark spot in the amorphous matrix. The spe contrast of the matrix also strongly changes with the imaging conditions. Fig. 8 is to the influence of relaxation on the HREM image contrast of the small crystalline cub and cuboctahedral silver particles in glass. The micrographs are calculated for the de of −70 nm, for which the lattice fringe contrast is enhanced. Comparing the unre particles with the relaxed ones reveals disturbances in the surface and a reduction image contrast of the relaxed particles in addition to the Fresnel fringes at the pa border and the speckled glass contrast. For the underfocus of −36.7 nm and for diff orientations the image contrast of both an unrelaxed and a relaxed spherical silver pa is shown in Fig. 9. Starting off in an (011) orientation the particle is turned around up to 10°. The contrast of the relaxed particle seems to be less extended than that unrelaxed one. With the rotation angle increasing, the image contrast of the particl be disturbed, but even at rotation angles up to 10° the lattice fringes of the precipitat clearly be detected. These investigations, carried out also with other orientations and yie similar results, suggest that most crystalline silver particles in commercial glasses sh be detectable by HREM.

4. Results and Discussion

The MD simulations demonstrate that relaxation effects of Ag particles in a glass m can be described by using plausible atomic potentials. The numerical results, how strongly depend on the particular forces and parameters applied. Nevertheless, Lennard-Jones potential cannot correctly explain the metallic bonds. The free Ag part show a relaxation behaviour completely different from that of particles enclosed in glass. Fig. 6 summarizes the results for cuboctahedral and spherical precipitates, embe in two slightly different glass models, as well as for free particles of different size. For free particles the lattice parameter increases with decreasing particle size (prob nonrealistic due to the Lennard-Jones potential used), whereas embedded particles s an opposite behaviour. The obvious influence of the matrix results in an additional pres on the particle. Relaxation calculations using better atomic potentials are necessar quantify this effect and to explain the energetic relations as a function of the interat forces.

The HREM simulations demonstrate the possibility of visualizing the relaxation eff Fig. 9 shows a good particle contrast at a large rotation angle, with the calculated fr distances not remarkably changing by rotation, but with the relaxation, however, stro influencing particle shape and fringe distances. This behaviour is quantitatively discu using diffraction patterns dynamically calculated in Fig. 10a, which were compared v geometrical reflection positions according to the strike length of the Ewald construc (Fig. 10b). The diffraction patterns refer to the particle contrast discussed in Fig. 9, for e (011) orientation (Fig. 10a, 0°) and for 10° rotation around the ($1\bar{1}1$) axis. Comparin

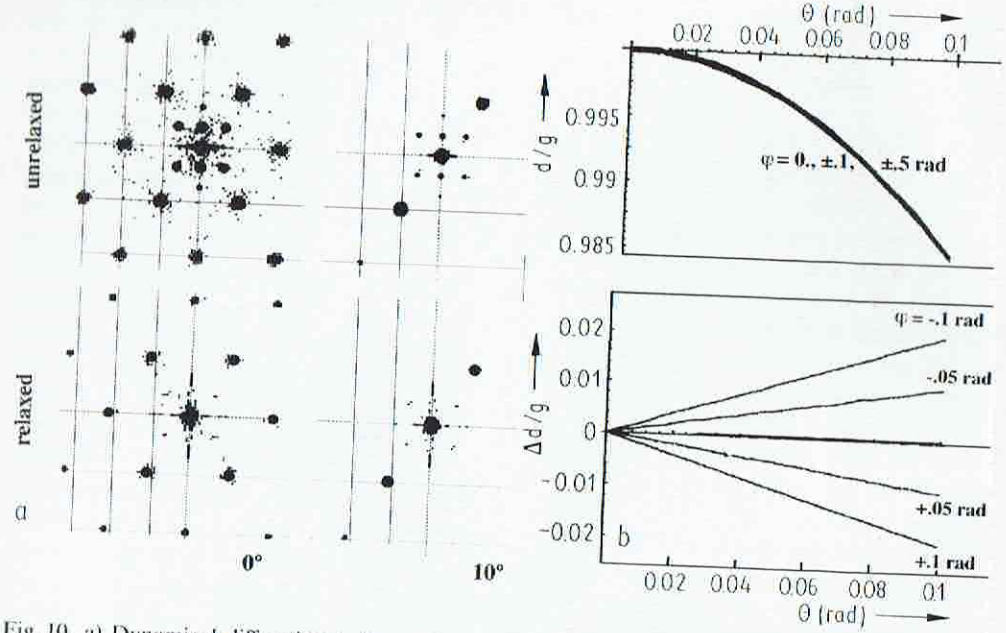

Fig. 10. a) Dynamical diffraction patterns ($\theta = 0°$, 10°) calculated for a spherical (011) oriented Ag particle (1722 atoms) before (upper row) and after relaxation (lower row), and b) geometrical reflection positions (peak location according to the geometrical strike length, distances $\Delta d/g$ and mean value d/g of opposite reflections g) as a function of surface inclination φ and beam tilt θ

with 10° does not reveal any influence of the peak position on the rotation of the particle. A remarkable effect, however, occurs, if the unrelaxed structure is compared with the relaxed one in the upper and lower rows, respectively, of Fig. 10a. The geometrical strike length (see Fig. 10b) is given by the excitation error

$$s = -[g^2 - Kg \sin(2\theta)]/2[K \cos(\theta + \varphi) + g \sin(\varphi)]$$

for reflection g and wave vector K from the literature; it will be discussed in detail elsewhere. The angle θ characterizes the beam tilt with respect to a symmetric high-order Laue zone orientation excited, whereas φ describes the angle between the surface normal and the symmetric position. In a first-order approximation, neglecting the reciprocal thickness effect for $s \approx 0$, the projection of s onto the Ewald construction sphere gives an upper limit of the shifts of the geometrical peak positions, here plotted as the mean value d/g of the opposite $\pm g$ reflections and the corresponding difference $\Delta d/g$. The mean value d/g corresponds to the reciprocal lattice fringe distance of first order and is almost independent of the surface inclination. The difference $\Delta d/g$ characterizes the second-order (non-linear) images. If beam tilt and surface inclination are geometrically affected this will not be reflected in the simulated dynamical diffraction patterns whereas the lattice contraction owing to particle relaxation becomes clearly visible as enlarged reflection distances.

5. Conclusions

Relaxation effects of Ag particles in a glass matrix can be under

calculations by MD and subsequent HREM image simulations. While particle rotation solely causes minor changes of the lattice fringe distances, the relaxation behaviour is clearly revealed by HREM.

Acknowledgements

The authors are very thankful to Dr. H. Hofmeister (MPI Halle), Dr. M. Dubiel, and Dr. K.-J. Berg (University Halle) for cooperation and discussion, and to the DFG and Stiftung Volkswagenwerk for financial support.

References

[1] K.-J. Berg, A. Berger, and H. Hofmeister, Z. Phys. D **20**, 313 (1991).
[2] M. Dubiel, H. Hofmeister, and St. Thiel, Detection and Characterization of Silver Particles in Sodium Silicate Glasses by Means of High Resolution Electron Microscopy, in: Physics and Chemistry of Finite Systems: From Clusters to Crystals, Vol. II, Ed. P. Jena, S. N. Khanna, and B. K. Rao, Kluwer Academic Publ., Dordrecht 1992 (pp. 1071 to 1076).
[3] K. Scheerschmidt and D. Timpel, Optik **93**, Suppl. 5, 81 (1993).
[4] K. Scheerschmidt and D. Timpel, Proc. 13. ICEM, Paris, 1994, Vol. 2A (p. 395).
[5] M. W. Finnis and J. E. Sinclair, Phil. Mag. **A50**, 45 (1984).
[6] G. J. Ackland and R. Thetford, Phil. Mag. **A56**, 15 (1987).
[7] G. J. Ackland, G. Tichy, V. Vitek, and M. W. Finnis, Phil. Mag. **A56**, 735 (1987).
[8] F. H. Stillinger and T. A. Weber, Phys. Rev. B **31**, 5262 (1985).
[9] J. Tersoff, Phys. Rev. Letters **56**, 632 (1986).
[10] J. Tersoff, Phys. Rev. B **37**, 6991 (1988).
[11] S. H. Garofalini, J. non-crystall. Solids **120**, 1 (1990).
[12] CERIUS, a Program Package for MD Calculation Molecular Simulations Incorporation, St.-John's Innovation Centre, Cambridge (UK).
[13] R. Schmitz, Diploma work, Halle 1993.
[14] S. Giorgio and J. Urban, J. Phys. F **18**, 147 (1988).
[15] H. Hofmeister, M. Dubiel, H. Goj, and St. Thiel, Proc. 13. ICEM, Paris, 1994, Vol. 2A (p. 401).
[16] P. A. Stadelmann, Ultramicroscopy **21**, 131 (1987).